Available online at www.sciencedirect.com

ScienceDirect

Publishing Services by Elsevier

International Journal of Naval Architecture and Ocean Engineering 8 (2016) 456–465

http://www.journals.elsevier.com/international-journal-of-naval-architecture-and-ocean-engineering/

# Numerical study on Wells turbine with penetrating blade tip treatments for wave energy conversion

Ying Cui, Beom-Soo Hyun*

*Division of Naval Architecture and Ocean Systems Engineering, Korea Maritime and Ocean University, Busan, South Korea*

Received 23 November 2015; accepted 30 May 2016
Available online 16 July 2016

**Abstract**

In order to optimize the performance of a Wells turbine with fixed guide vanes, the designs of an end plate and a ring on the tip of the turbine rotor are proposed as penetrating blade tip treatments. In this study, numerical investigations are made using computational fluid dynamics (CFD)-based ANSYS Fluent software, and validated by corresponding experimental data. The flow fields are analyzed and non-dimensional coefficients $C_A$, $C_T$ and $\eta$ are calculated under steady-state conditions. Numerical results show that the stalling phenomenon on a ring-type Wells turbine occurs at a flow coefficient of $\phi = 0.36$, and its peak efficiency can reach 0.54, which is 16% higher than that of an unmodified turbine and 9% higher than in the case of an endplate-type turbine. In addition, quasi-steady analysis is used to calculate the mean efficiency and output work of a wave cycle under sinusoidal flow conditions. As a result, it has been found that the ring-type turbine is superior to other types of Wells turbines.



*Keywords:* Oscillating water column (OWC); Wells turbine; Computational fluid dynamics (CFD); Blade tip treatment; Endplate-type rotor; Ring-type rotor; Steady & quasi-steady analysis

## 1. Introduction

Among various renewable energy sources, wave energy from the oceans is one of the most promising. A series of technologies has been developed to extract energy from waves and convert it to mechanical energy or electric energy, such as the Oscillating Water Column (OWC), the overtopping system, the floating buoy, the point absorber, and the tapered channel (TAPCHAN) device. In recent times, the OWC wave energy converter has been widely utilized to harness wave energy, such as the 500 kW LIMPET in the UK, the 500 kW PICO in Portugal, and the 2 × 250 kW Yongsoo in South Korea (Cruz, 2008). The OWC system has a large chamber to take in incident waves and generate the oscillating water column. Then, the pressure difference between the atmosphere and the chamber compresses the air to exhale and inhale through the air turbine. As the essential part for the second energy conversion stage, air turbines are capable of converting low pressure pneumatic energy into mechanical shaft power. The most popular self-rectifying air turbines include the impulse turbine and the Wells turbine. Both can rotate in one direction through the pivot under bi-directional air flows. Since the impulse turbine was proposed by Kim et al. (1988), an agreement has been gradually reached that it has several advantages over the Wells turbine in terms of a wider operating flow range, better self-starting performance, and lower working noise. While, the Wells turbine, which was proposed by Wells in 1976 (Raghunathan, 1985), has higher operating efficiency, lower expense on fabrication and maintenance, and is more suitable for a higher rotational regime. Hence, enhancing its operating performance will play a crucial role in increasing the efficiency of wave energy conversion for an

* Corresponding author.
*E-mail address:* bshyun@kmou.ac.kr (B.-S. Hyun).
Peer review under responsibility of Society of Naval Architects of Korea.

http://dx.doi.org/10.1016/j.ijnaoe.2016.05.009

**Nomenclature**

| | |
|---|---|
| $b$ | blade height |
| $C_A$ | input coefficient |
| $C_T$ | torque coefficient |
| $D$ | duct diameter |
| $f$ | circular frequency of rotor blade |
| $G$ | gap between guide vane and rotor blade |
| $l_a$ | axial length of rotor blade |
| $l_g$ | chord length of guide vane |
| $l_r$ | chord length of rotor blade |
| $Q$ | air flow rate |
| $r_R$ | mean radius of blade |
| $Re$ | Reynolds number |
| $T$ | wave period |
| $T_0$ | turbine output torque |
| $U_R$ | circumferential velocity at $r_R$ |
| $v_a$ | mean axial flow velocity |
| $V_a$ | peak value in sinusoidal flow |
| $W$ | output-work of a wave cycle |
| $y$ | distance from the wall to cell center |
| $z$ | number of rotor blades |
| $\Delta p$ | total pressure drop between setting chamber and atmosphere |
| $\phi$ | flow coefficient |
| $\Phi$ | flow coefficient under sinusoidal flow condition |
| $\gamma$ | stagger angle of guide vanes |
| $\eta$ | turbine efficiency |
| $\overline{\eta}$ | mean turbine efficiency under sinusoidal flow condition |
| $\theta$ | chamber angle of guide vane |
| $\rho_a$ | air density |
| $\mu$ | molecular viscosity |
| $\tau_w$ | wall shear stress |
| $\nu$ | hub-to-tip ratio |
| $\omega$ | angular velocity of turbine rotor |

OWC plant, and help overcome the fossil fuel crisis consequently.

Several researchers have explored the pneumatic characteristics of air turbines with experimental and numerical methods. The basic principle of improving their performances is changing the configuration of the blades or guide vanes with respect to the original design, and searching for the optimum geometry parameters. For an impulse turbine, a series of experiments, which was carried out by Setoguchi et al. (2001) and Takao and Setoguchi (2012), summarized years of research achievements, and provided optimum geometry parameters. Thakker and Dhanasekaran (2003, 2005) and Thakker et al. (2005) systematically established three-dimensional (3-D) numerical models to explore the effects of tip clearance, guide vane losses, and guide vane shapes, respectively. It was reported that an optimum tip clearance of 0.25%D was suggested wherein the effect of tip leakage flow was almost negligible. Inspired by the winglet of an airplane, Hyun et al. (2005) first applied the design of an end plate to an impulse turbine, and investigated the performance of this special-type turbine at various design parameters using the numerical method. Results showed that a penetrating end plate increased the turbine efficiency due to a decrease in the input coefficient. Meanwhile, a so-called ring-type impulse turbine was also proposed and analyzed numerically to minimize the adverse effects of tip clearance by Hyun et al. (2006). Hence, it is reasonable to expect that applying an end plate or ring to a Wells turbine could improve the operating performance. In addition, Cui et al. (2015a) proposed a staggered turbine with a positive setting angle of rotor blades, which was numerically proved to be superior to the original design for the case of asymmetrical air flows.

For Wells turbine, a research by Raghunathan (1995) revealed that a decrease in tip clearance advanced the stall but increased efficiency as a result of reduced leakage losses. A turbine with a relatively large tip clearance could operate over a much wider range of flow coefficients without stalling. Several experiments were performed by Takao et al. (2001) and Setoguchi et al. (2003b). Their reports described the effects of guide vanes and rotor geometry. It was concluded that the guide vane contributed to postpone stalling, improving the turbine efficiency and the starting and transitional characteristics under running conditions. And the NACA four digit series with the thickness ratio of 20% was found to be a suitable choice for the blade profile of the Wells turbine. A modified Wells turbine, which has a positive setting angle of blades, was also shown to fit the asymmetric profile of flow rate with better performance characteristics (Setoguchi et al., 2003a). Kim et al. (2002a, 2003) employed numerical simulation to study the hysteretic characteristics and the effects of blade sweep. The numerical model was well validated to predict the performance of a Wells turbine without guide vanes, which provides the reference to the numerical simulation in this paper. Takao et al. (2006) applied the end plate to a Wells turbine without guide vanes, and experimentally studied the effects of plate size, plate type, and tip clearance. Results revealed that the attribution of the end plate existed in an increase in the torque coefficient. Mohamed et al. (2011) and Mohamed and Shapaan (2014) numerically optimized the airfoil shape to increase the tangential force, and studied the effects of blade pitch angle on improving the turbine efficiency. Finally it is worth noting that Halder et al. (2015) recently investigated the effects of blade tip clearance and a tip penetrating depth into casing on the performance of Wells turbine. They showed that the penetrating depth of 3% of the chord length produced highest power and widest operating range.

According to the study by Thakker and Dhanasekaran (2003), minimizing the adverse effects of tip clearance improved the turbine efficiency. Hence, the geometry of a blade penetrating into the duct is expected to reduce the tip clearance compared to the original turbine. And in the wing system of an airplane, the induced drag is generated by the distribution of lift across the wing, and is strongly influenced by tip vortices. Then the winglets are designed to reduce the strength of tip vortices and therefore cause the flow across the wing to be more two-dimensional (2-D) with less induced

drag. Moreover, the geometry of a ring housed in the duct has been applied to some special-purpose marine vehicles. Borrowed from the concepts of winglets and ring, two configurations of penetrating end plate and penetrating ring are proposed for the Wells turbine with fixed guide vanes in this paper. Numerical simulation is carried out using the commercial CFD software ANSYS Fluent. The geometry and grids are generated in the pre-processing Software Gambit. Based on verification with corresponding experimental data, 3-D calculations are performed under steady flow conditions in order to determine the optimum structure. The numerical results are shown by means of dimensionless coefficients, contours of velocity, and velocity streamlines. Then quasi-steady analysis is employed to compare the two modified turbines with the original design in terms of mean efficiency and output work of a wave cycle. As a result, it has been found that the penetrating ring-type Wells turbine is superior to the other types, and is thereby recommended for future applications in OWC wave energy converters.

## 2. Turbine geometry

In this study, the original geometry of a Wells turbine with 2-D fixed guide vanes refers to the recommendation by Takao et al. (2001). The turbine has a diameter ($D$) of 300 mm and a hub-tip-ratio $\nu$ of 0.7. Fig. 1 illustrates the 3-D sketch and detailed profiles of the original turbine. There are six rotor blades and eleven guide vanes. As suggested by Setoguchi et al. (2003b), the blade profile of NACA0020 is selected with a chord length of $l_r = 90$ mm. The tip clearance between the rotor and the duct is 1 mm. Guide vanes with the chord length of $l_g = 91$ mm are symmetrically installed at a distance ($G$) of 39 mm downstream and upstream of the rotor. The profile of the guide vanes is a circular arc with a chamber angle of $\theta = 60°$ and a stagger angle of $\gamma = 16.3°$. The leading and trailing edges are rounded to a semicircle with a radius of 0.5 mm. The specifications of the original turbine model are summarized in Table 1. Based on this original turbine, the end plate or ring with a thickness of 0.5 mm is installed at the tip of the rotor blades in order to minimize the adverse effects of leakage flow in the tip region. For comparison, some sectional geometry dimensions of the end plate and ring are set identically. Hence, the axial length of end plate and ring are both 15% larger than that of the original rotor blade, and the end plate has a shape similar to the blade section. In addition, the penetration has an axial width of 23 mm and a depth of 1 mm. Fig. 2 clearly shows the geometric differences of the three turbines in terms of the 3-D schematic layout, dimensions, and the section of the rotor and duct. The two dashed areas stand for the walls of the hub and duct, respectively. The narrow area (black) is the end plate or ring at the tip of the rotor blade, which penetrates into the duct. The basic form of the endplate-type Wells turbine, including the plate size, the plate position, and the tip clearance, comes from the report by Takao et al. (2006).

Table 1
Specification of the turbine model.

| Rotor blade profile | NACA0020 |
|---|---|
| Number of blades | 6 |
| Chord length of rotor blade | 90 mm |
| Solidity of rotor blade | 0.67 |
| Guide vane profile | Circle arc |
| Number of guide vanes | 11 |
| Chord length of guide vane | 91 mm |
| Solidity of guide vane | 1.25 |
| Stagger angle of guide vane | 16.3° |
| Chamber angle of guide vane | 60° |
| Duct diameter | 300 mm |
| Hub diameter | 210 mm |
| Mean radius | 127.5 mm |
| Gap between guide vane and rotor blade | 39 mm |
| Tip clearance | 1 mm |

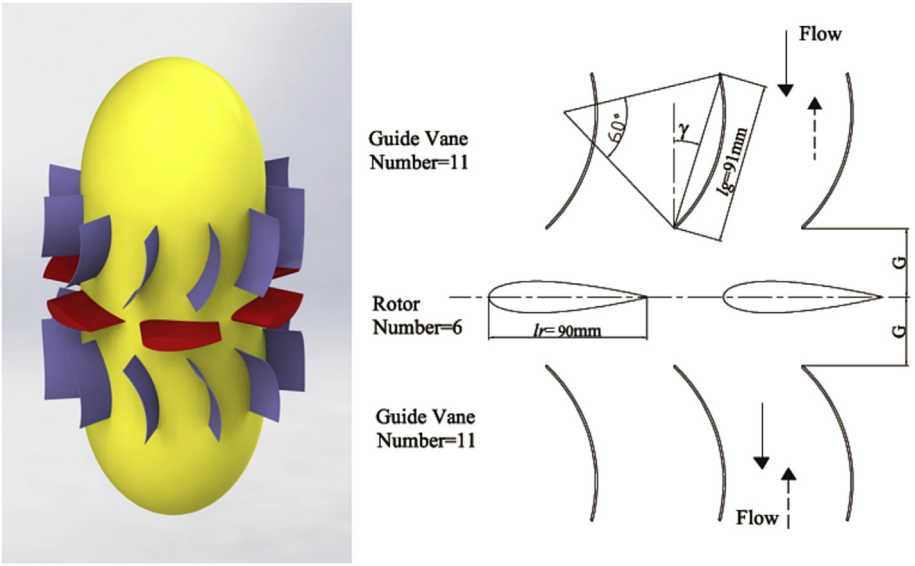


Fig. 1. 3D sketch and turbine configuration at mean radius.

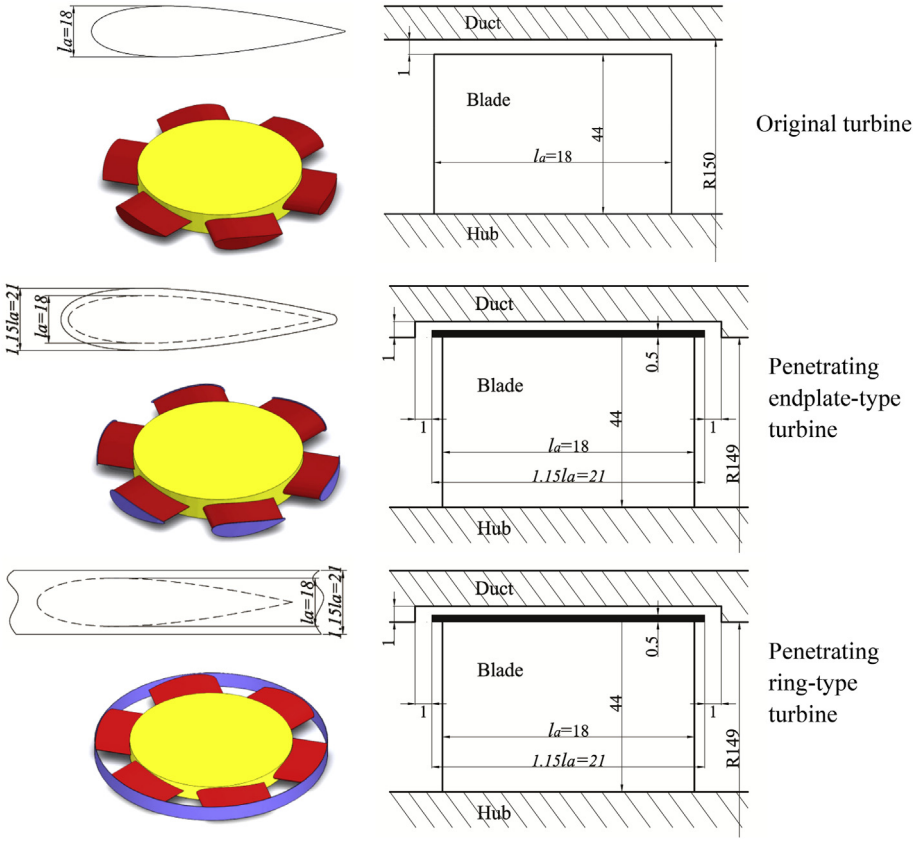


Fig. 2. Geometric comparison of three turbines.

## 3. Pneumatic performance evaluation

According to the study by Takao et al. (2001), four dimensionless coefficients are used to evaluate the performance of turbines under steady flow conditions: the input coefficient $C_A$, the torque coefficient $C_T$, the turbine efficiency $\eta$, and the flow coefficient $\phi$. The definitions are listed in the following:

$$C_A = \frac{2\Delta pQ}{\rho_a\left(v_a^2 + U_R^2\right)bl_r z v_a} \tag{1}$$

$$C_T = \frac{2T_0}{\rho_a\left(v_a^2 + U_R^2\right)bl_r z r_R} \tag{2}$$

$$\eta = \frac{T_0\omega}{\Delta pQ} = \frac{C_T}{C_A\phi} \tag{3}$$

$$\phi = v_a/U_R \tag{4}$$

where $\Delta p$, $Q$, and $T_0$ represent the total pressure drop between two sides of the turbine, the air flow rate, and the generated torque, respectively; $\rho_a$, $b$, and $z$ are the air density, the blade height, and the number of rotor blades, respectively. $v_a$, $r_R$, $\omega$, and $U_R$ mean the axial flow velocity, the mean radius, the angular velocity of the turbine, and the circumferential velocity at $r_R$, respectively.

The quasi-steady analysis, which has been validated by previous studies (Inoue et al., 1986), is employed to simulate the running characteristics of a Wells turbine under oscillating air flows. In addition, the report by Hyun et al. (2007) indicated that the quasi-steady method provided a practical and useful way to predict the operating performance of impulse turbine under sinusoidal flow conditions. First, the wave frequency is low enough when compared to the impulse turbine's rotating frequency, so the interaction between the wave and turbine can be neglected, and the air flow can be assumed to be quasi-steady. Second, since the reduced frequency $(fl/(v_a^2 + U_R^2)^{1/2})$ is on the order of magnitude of $10^{-3}$, the amplitude attenuation and phase lag of the unsteady flow can be ignored. Meanwhile, it is noted that the Wells turbine has a smaller reduced frequency due to the higher rotating velocity. Hence, it is efficient to apply the quasi-steady method to the unsteady problem with the steady performance coefficients computed; this greatly reduces the time consumption of fully unsteady calculations with sufficient accuracy. For simplicity, the axial velocity through the turbine is described ideally as a sinusoidal pattern, as shown in Fig. 3. When the turbine is in the running condition, all the parameters of turbine characteristics such as $T_0$, $\omega$, $\Delta p$, and $Q$ vary periodically for real conditions. In this case, the operating performance is characterized by the mean efficiency $\overline{\eta}$ and flow coefficient $\Phi$, which can be defined by the following equations:

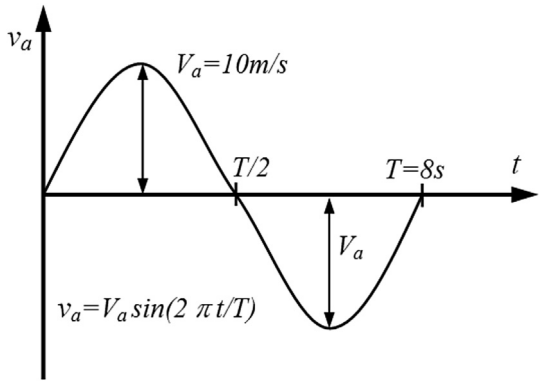


Fig. 3. Axial velocity variation with time.

$$\overline{\eta} = \frac{\frac{1}{T}\int_0^T T_0 \omega dt}{\frac{1}{T}\int_0^T \Delta p Q dt} \tag{5}$$

$$\Phi = V_a / U_R \tag{6}$$

Furthermore, an output work analysis is conducted to compare the operating performance of different turbines more practically. An expression for the total output work within a wave period is derived from Eq. (2) using $W = \int_0^T T_0 \omega dt$ and $\phi = \Phi \sin(2\pi t/T)$ as follows:

$$W = \frac{1}{2}\rho_a b l_r z V_a^3 \int_0^T C_T \left(\frac{1}{\Phi^3} + \frac{1}{\Phi}\sin^2\left(\frac{2\pi}{T}t\right)\right) dt \tag{7}$$

where $V_a$ and $T$ are the amplitude and wave period of the sinusoidal flow velocity, respectively. In the calculations, the flow condition is assumed to be quasi-steady; therefore, the values of $C_A$ and $C_T$ under steady conditions are used. Then, the integrations included in Eqs. (5) and (7) are carried out using the data-processing software Matlab with the given steady characteristics and a certain flow coefficient $\Phi$. Furthermore, the presentation of calculation results is completed in post-processing software Tecplot.

## 4. Numerical method

ANSYS Fluent is applied in the numerical simulation, which uses the finite volume method to solve Reynolds-Averaged Navier–Stokes equations by employing a pressure-based solver. The SIMPLEC scheme is used for the pressure–velocity coupling, which has a faster speed of convergence than the SIMPLE scheme. The second order upwind scheme is used for the spatial discretization. In addition, the realizable k-ε turbulence model is chosen with the standard wall function to process the turbulent effects for the Wells turbine. The mixing plane (MP) model is adopted to deal with the number difference between the guide vanes and blades. The axial velocity at the velocity inlet boundary is kept constantly, and the revolutions per minute (RPM) of the rotor blade is varied to generate the range of the flow coefficient.

The geometry and grids are generated with the pre-processing Software Gambit. As shown in Fig. 4, a hybrid mesh is created with Map-Hex mesh near the rotor and Tri-Pave mesh in the other regions. Grids cluster near the blade and guide vanes, and gradually thin out. There are four grids in the span-wise direction in the tip clearance region to capture the detailed flow property. The non-dimensional parameter Y+ $\left(\text{Y+} = \frac{\nu}{\mu}\sqrt{\rho_a \tau_w}\right)$ is used to define the locations of the wall's adjacent cells to ensure that the cells lie in an appropriate distance away from the wall. The value of Y+ is dependent on the resolution of the mesh and the Reynolds number. In the numerical study by Kim et al. (2002a), the Y+ value was recommended to be greater than 15. On this basis, the Y+ in the present study ranges from 15 to 30. The Reynolds number based on the blade chord and tip velocity is approximately equal to $2.9 \times 10^5$.

The boundary conditions are given in Fig. 5. In order to ensure the sufficient development of flow, the computational domain is extended by four and eight blade chord lengths upstream and downstream of the blade, respectively. The domain is divided into three parts: the upstream guide vane domain, the rotor blade domain, and the downstream guide vane domain. The guide vane domains are stationary, while the rotor domain is assumed to rotate at a constant speed. Moreover, the velocity inlet and pressure outlet boundary conditions are set at two opposite ends of the computational domain. Then, rotationally periodic boundaries are employed to create a numerical model with a single blade and two symmetric guide vanes without the computational expense of modeling all the rotors and stators; this will reduce the grid size and computing time to some degree. The mixing plane interfaces locate between the stationary and the rotating domains for all flow-field data exchanging. In the MP model, each fluid zone is solved as a steady-state problem. Flow-field data from the adjacent zones are passed as boundary conditions that are spatially mixed at the interfaces. After each iteration, the flow data at the interfaces are averaged circumferentially, and reasonable approximations of the time-averaged flow field are provided for the next iteration. The numerical method refers to the works of Cui et al. (2015a, 2015b).

Prior to studying the effects of the end plate and ring, the numerical model of the original Wells turbine with fixed guide vanes is validated with corresponding experimental data, which is extracted from the paper published by Takao et al. (2001). The basic geometry dimensions are the same as those in Fig. 1. For grid independency study, three grid sizes are tested for comparison: a coarse mesh ($4.1 \times 10_5$ cells), a medium mesh ($5.0 \times 10_5$ cells), and a fine mesh ($5.3 \times 10_5$ cells). The choice of the aforementioned cell numbers is based on previous experience and the literature (Kim et al., 2002a). Meanwhile, 16 flow coefficients are evaluated for each model to obtain continuous curves of numerical results: 0.1, 0.15, 0.2, 0.25, 0.3, 0.33, 0.34, 0.35, 0.36, 0.37, 0.4, 0.5, 0.6, 0.7, 0.8, and 1. In order to clearly simulate the stalling phenomenon,

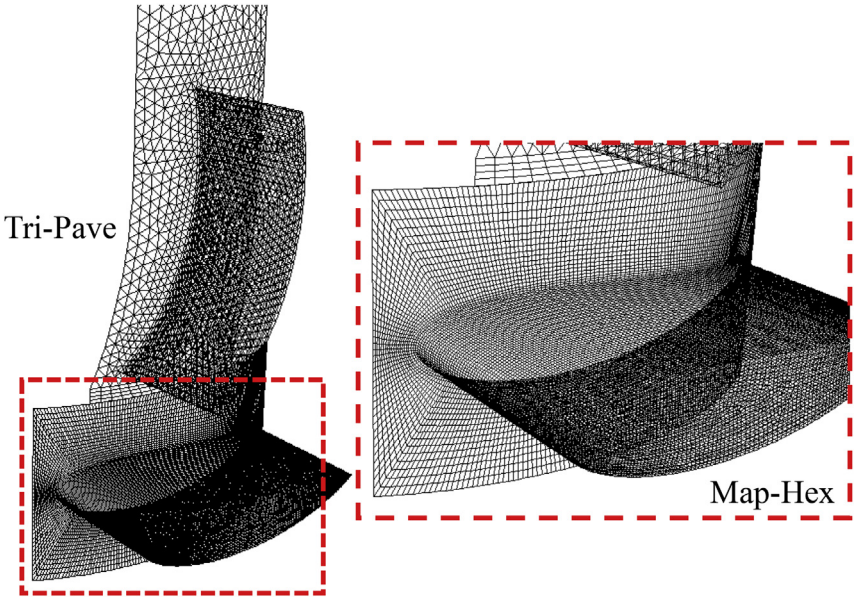


Fig. 4. Mesh structures of original Wells turbine with fixed guide vanes.

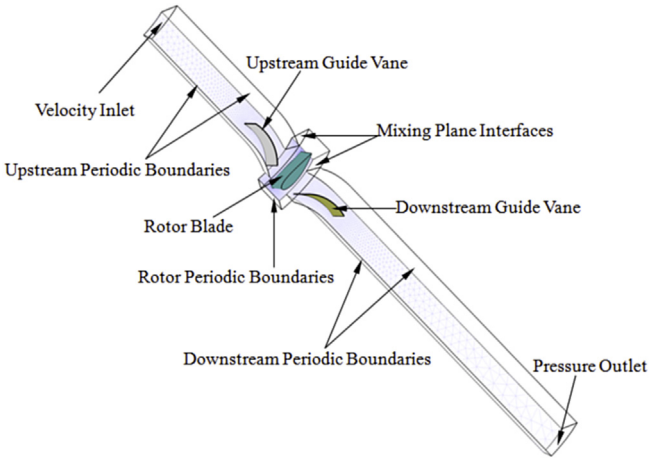


Fig. 5. Boundary conditions.

the intervals of flow coefficients near 0.35 are smaller than those of the other regions. Furthermore, four different turbulent models with various wall functions are compared for turbulent model test: Realizable $k$-$\varepsilon$ model with standard wall function, Standard $k$-$\varepsilon$ model with standard wall function, Realizable $k$-$\varepsilon$ model with non-equilibrium wall function, and SST $k$-$\omega$ turbulent model with specific wall treatment.

As presented in Fig. 6, experimental and numerical data of the input coefficient, the torque coefficient, and the turbine efficiency under steady conditions are compared. It can be seen from Fig. 6(a) that tiny differences exist among the three numerical curves of $C_A$, and the numerical predictions all agree well with experimental results at lower flow coefficients. However, when $\phi$ becomes higher ($\phi > 0.35$), the numerical calculations overestimate $C_A$ to some degree. A sudden fall, which is called "stalling", can be observed in Fig. 6(b) and (c) when the flow coefficient is equal to 0.35. Namely, when the angle of attack is higher than 19.3°, stalling occurs. This phenomenon results in a sudden loss of lift force for the rotor blades, and a subsequent drop in the values of $C_T$ and $\eta$. Before the stalling position, it is shown that the numerical results match well with experimental data. And the stalling position and maximum turbine efficiency (0.48) are also well predicted by the models with medium and fine meshes. However, the model with a coarse mesh has certain limitations in simulating the values of $C_T$ and $\eta$ near the stalling position. What's more, due to the complex phenomenon after stalling, the values of $C_T$ are overestimated, and the gap has an increasing tendency with the flow coefficient. The combined effects of the higher values of numerical $C_A$ and $C_T$ make $\eta$ agree well with the shape plotted by the experimental data. After stalling, the efficiency remains at a low level less than 0.07. On the other hand, the medium mesh requires 45 min−1 h to be converged under 3-cores parallel computational condition in Fluent. And the fine mesh spends more than almost twice computational time cost of the medium mesh. As for the turbulent model test, Fig. 6(d) shows that the best agreement with the experiment is achieve by the Realizable $k$-$\varepsilon$ turbulent model with standard wall function. The largest deviation from the experimental data is observed in the SST $k$-$\omega$ turbulent model.

Taking all of the comparisons into account, the medium mesh using the Realizable $k$-$\varepsilon$ turbulent model with standard wall function can effectively predict the stalling and peak efficiency with an acceptable accuracy and time cost. Hence, the numerical model established in this present work can be considered sufficiently reliable for the following study of the end plate and ring.

## 5. Results and discussion

Fig. 7 describes the velocity contours on the plane through 93% of the blade height ($b$), and the velocity streamlines on the suction surface when $\phi$ is equal to 0.2. As shown in Fig. 7(a), a

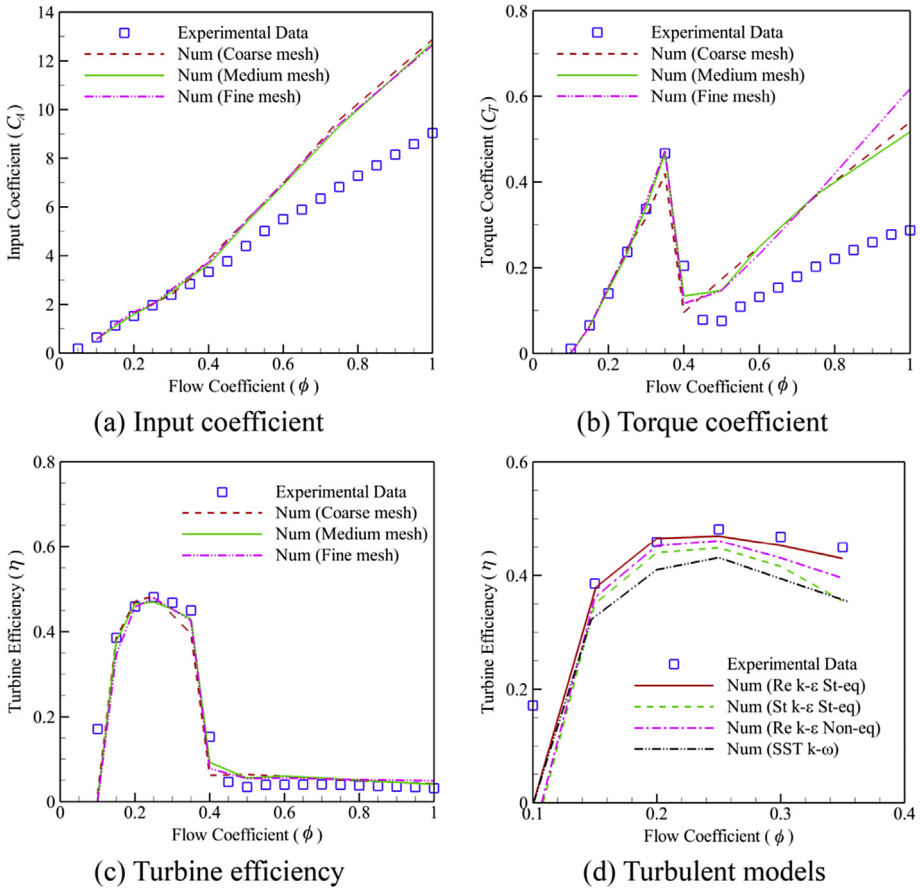


Fig. 6. Experimental validation for Wells turbine with guide vanes.

stagnation point locates in the forepart of the pressure side. On the suction side, dense contour lines emerge near the leading edge, which has larger velocity magnitude due to the end plate and ring. Then this high-velocity region begins to dissipate along the suction side. Since a strong interaction exists between the wake and the boundary layer, evident separation occurs from the middle of the suction side. Low pressure appears in this region, which is colored in blue in the figure. By comparison, it is found that the existence of the end plate or ring postpones the development of the separation, reduces the area of the separation region, and makes the region fit better with the trailing edge of the suction side. On the other hand, in Fig. 7(b), the streamlines drawn from the velocity vectors have more obvious differences. A vortex appears near the middle of the hub surface for the original turbine, and gradually diminishes and moves to the leading part because of the end plate and ring. On the tip side of the rotor blade, it is obviously observed that the end plate and ring can hinder the flow from passing through the edge near the tip. This results in the decrease of adverse effects of tip clearance, and contributes to improving the turbine performance to some extent.

A comparison of the three Wells turbines in terms of dimensionless coefficients is shown in Fig. 8. To clearly present the effects of the end plate and ring before stalling, the x-coordinates in Fig. 8(a) and (b) are set from 0 to 0.4. In Fig. 8(a), it is shown that within this range, the input coefficient $C_A$ shows a generally upward trend with the flow coefficient, and the end plate or ring can decrease the value of $C_A$ to a very small degree. Fig. 8(b) indicates that the ring-type turbine has better performance in terms of increasing $C_T$, and the stalling position is shifted slightly from $\phi$=0.35 to 0.36. While, there is only a very slight difference in terms of the stalling position and the peak value between the curves of the endplate-type and original type; this reveals that the penetrating end plate has no influence in improving the torque coefficient $C_T$. Furthermore, the trends of turbine efficiency $\eta$ are similar for the three turbines, as shown in Fig. 8(c). When the flow coefficient $\phi$ changes from 0.1 to 0.2, $\eta$ increases rapidly until peak efficiency is reached. Then a slow decrease appears until the sudden drop at the stalling position. The value of turbine efficiency after stalling is too small to have practical significance. The comparison of turbine efficiency demonstrates that the Wells turbine with a penetrating ring is optimum. The maximum efficiency of the ring-type turbine is 0.54 at $\phi = 0.2$, which is 16% higher than that of original design and 9% higher than in the case of the endplate-type. And the effect of the end plate is relatively small with an average improvement of 6% in turbine efficiency $\eta$ over the original design. However, in the report by Cui et al. (2015b), it was concluded that for a Wells turbine without guide vanes, the endplate-type showed the optimum performance in postponing stalling and increasing the torque coefficient $C_T$ when compared with the ring-type

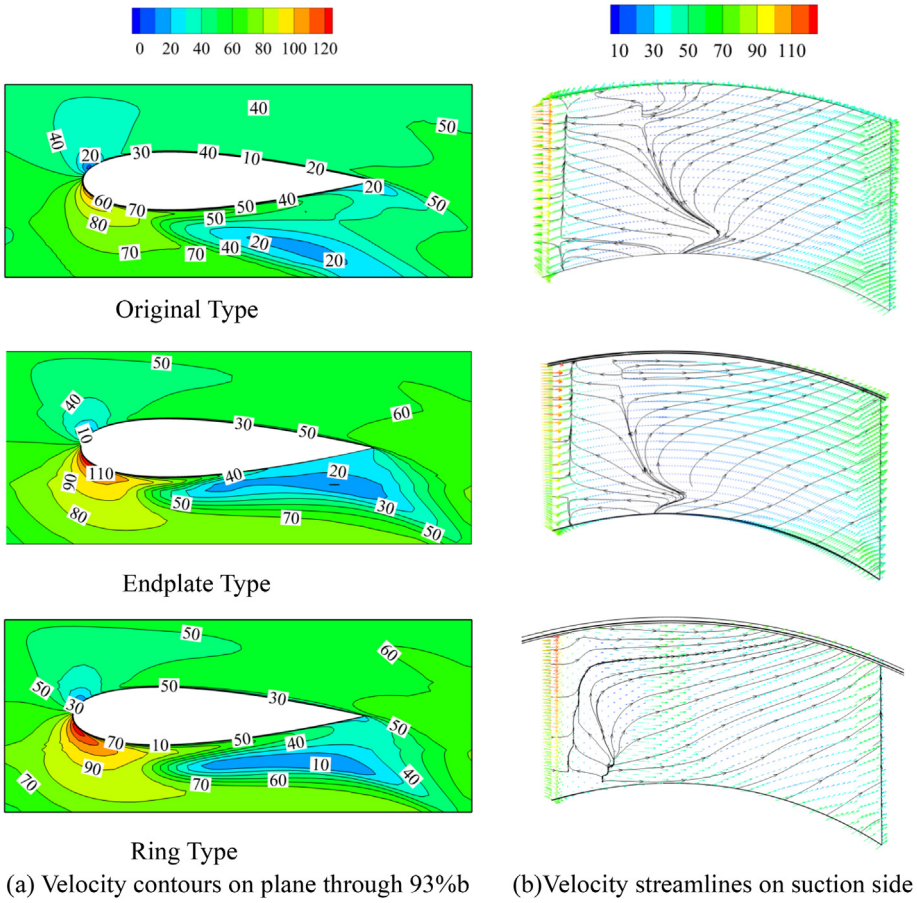


Fig. 7. Velocity contours and streamlines of Wells turbine ($\phi = 0.2$).

and original turbines. The stalling position of the endplate-type turbine is $\phi = 0.33$, and the maximum efficiency could be increased to 0.5. But the ring-type turbine had a narrower region of flow coefficient with the stalling position at $\phi = 0.25$. Since the end plate or ring was directly attached to the tip of the rotor blade without penetration in the study by Cui et al. (2015b), the difference may be caused by the existence of the penetration and guide vane. The specific reason should be studied further in future work.

In addition, the mean efficiency and output work of a wave cycle is calculated using Eqs. (5) and (7) in order to analyze the operating performance under sinusoidal flow conditions. As given in Fig. 9(a), the general shape of the mean efficiency is similar to that of turbine efficiency under steady flow conditions. The value is enhanced sharply when the flow coefficient $\Phi$ changes from 0.15 to 0.2, and keeps at a relatively stable level until the stalling position. Subsequently, the mean efficiency sharply drops to a small value because of the stalling phenomenon. It's obvious that the ring-type turbine has the highest mean efficiency of 0.49 at $\Phi = 0.3$, which is 17% greater than that of original type and 9% larger than in the case of the endplate-type. Moreover, Fig. 9(b) shows the output work of a wave cycle. The details of the wave cycle are shown in Fig. 3, including the period and amplitude of the wave cycle. The x-coordinate represents the revolutions per minute (RPM), which ranges from 0 to 3000. Even though the Wells turbine is suitable for a high rotational regime, an RMP speed larger than 3000 is not practical in real engineering. It can be observed that the maximum output work of the ring-type turbine is 1441 J at 2700 RPM, while that of the original or endplate type is 1230 J. When the RPM falls to 1700, the angle of attack increases and stalling occurs; this results in the steep decrease of output work. When the RPM is 1000, the values for the three turbines are only about 160 J.

The above results reveal that the modified geometry of a penetrating ring can improve the operating performance of an air turbine under steady or sinusoidal flow conditions, and should be recommended for the future applications on Wells turbines with fixed guide vanes.

## 6. Conclusion

In order to improve the performance of a Wells turbine, the geometries of penetrating ring-type and penetrating endplate-type turbines are proposed based on the original design with fixed guide vanes. 3-D numerical models of a Wells turbine are established using the CFD software ANSYS Fluent. The geometry and grids are generated using the pre-processing

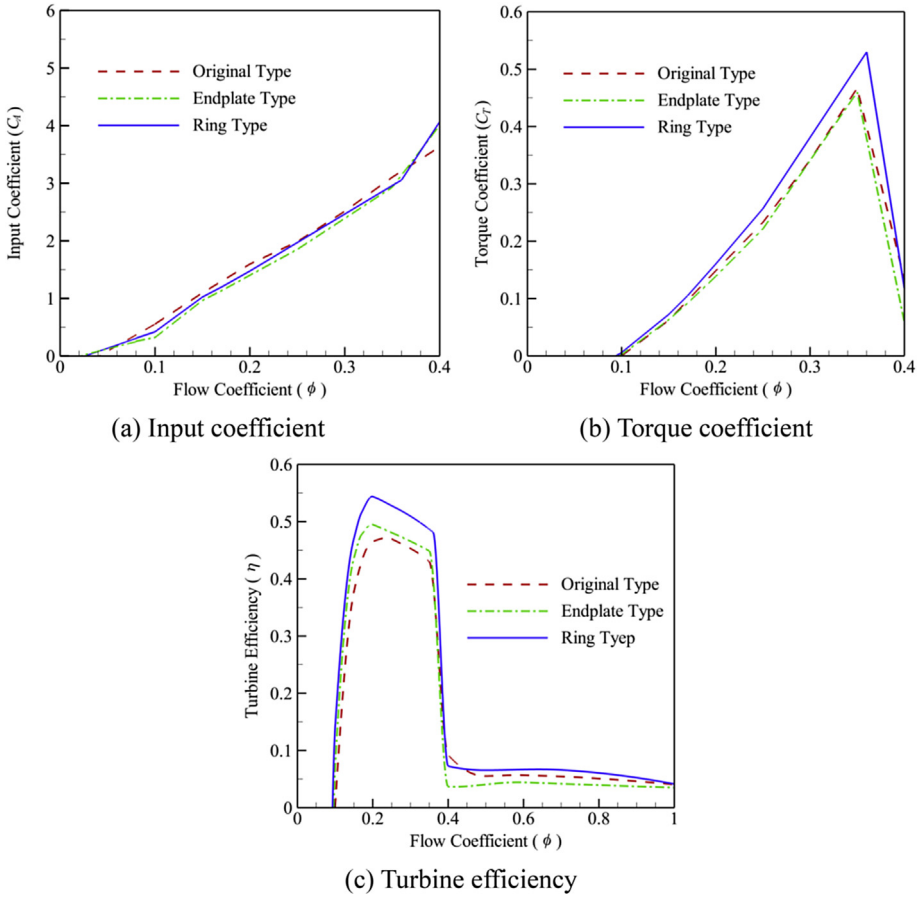


Fig. 8. Effects of end plate and ring on Wells Turbine.

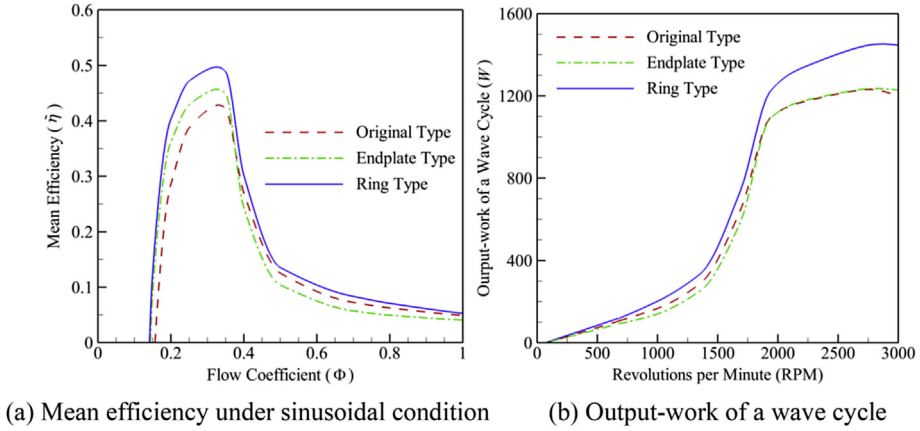


Fig. 9. Turbine performance under sinusoidal flow condition.

software Gambit. All calculations are performed for steady conditions. The models are primarily validated with corresponding experimental data.

Velocity contours, velocity streamlines on suction surfaces, and the dimensionless evaluating coefficients are obtained in order to analyze the effects of the end plate and ring. Conclusions can be drawn that compared with the original design and the penetrating endplate-type, the ring-type turbine is optimum for the case of unidirectional steady flow. The stalling position of a ring-type Wells turbine is $\phi = 0.36$, and the maximum efficiency is 0.54 at $\phi = 0.2$, which is 16% higher than that of original one and 9% higher than in the case of the endplate type. In terms of performance under sinusoidal flow conditions, the mean efficiency and output work of a wave cycle are compared among the three turbine configurations. The ring-type turbine has the highest mean efficiency of

0.49 at $\Phi = 0.3$, and a maximum output work of 1441 J at 2700 RPM within a wave period. Thus, the penetrating ring-type turbine is recommended as a better choice for a Wells turbine than other designs.

This work primarily explores the effects of a penetrating end plate and ring on the performance of a Wells turbine with guide vanes. However, the study on penetration is not complete. While some researches such as Halder et al. (2015) presented an extensive set of parametric study on rotor tip treatment, there may be more room for the optimization of a Wells turbine through a more rigorous investigation on sophisticated blade tip treatments. In addition, it is clarified by Kim et al. (2002b) that the hysteresis is closely related to the different behavior of blade wake between an increasing process and a decreasing process in the angle of attack. The quasi-steady analysis used in this present work neglects the effects of hysteresis on turbine performance in an oscillating flow. Hence, it is worth further studying the hysteresis characteristics of Wells turbine with end plate and ring to explore the advantages of this penetrating blade tip treatments.

## Acknowledgments

This work was supported by the Graduate School of the Korea Maritime and Ocean University.

## References

Cruz, J., 2008. Ocean Wave Energy – Current Status and Future Perspectives. Springer-Verlag, Berlin, p. 210.

Cui, Y., Liu, Z., Hyun, B.S., 2015a. Pneumatic performance of staggered impulse turbine for OWC wave energy convertor. J. Therm. Sci. 24 (5), 1–7.

Cui, Y., Liu, Z., Hyun, B.S., Kim, K.W., 2015b. Numerical study on comparison of steady performance between impulse and Wells turbines for wave energy conversion. In: Proceedings of the 7th Workshop for Marine Environment and Energy, Keelung, Taiwan.

Halder, P., Samad, A., Kim, J.H., Choi, Y.S., 2015. High performance ocean energy harvesting turbine design – a new casing treatment scheme. Energy 86, 219–231.

Hyun, B.S., Moon, J.S., Hong, K., Hong, S.W., 2007. Performance prediction of impulse turbine system in various operating conditions. J. Ocean Eng. Technol. 21 (5), 9–17.

Hyun, B.S., Moon, J.S., Hong, S.W., Kim, K.S., 2005. Design of impulse turbine with an end plate for wave energy conversion. In: Proceedings of the 15th International Offshore and Polar Engineering Conference, Seoul, Korea, 1, pp. 507–512.

Hyun, B.S., Moon, J.S., Hong, S.W., Kim, K.S., 2006. A study on the performance of the ring-type impulse turbine for wave energy conversion. J. Korean Soc. Ocean Eng. 20 (1), 20–25.

Inoue, M., Kaneko, K., Setoguchi, T., Raghunathan, S., 1986. Simulation of starting characteristics of the Wells turbine. In: ALAA/ASME 4th Fluid Mech Plasma Dyn Lasers Conf, AIAA-86-1122.

Kim, T.H., Setoguchi, T., Kaeneko, K., Raghunathan, S., 2002a. Numerical investigation on the effect of blade sweep on the performance of Wells turbine. Renew. Energy 25, 235–248.

Kim, T.H., Setoguchi, T., Kinoue, Y., Kaneko, K., Inoue, M., 2002b. Hysteretic characteristics of Wells turbine for wave power conversion. In: Proceedings of the 12th International Offshore and Polar Engineering Conference, Kitakyushu, Japan, 1, pp. 687–693.

Kim, T.H., Setoguchi, T., Kinoue, Y., Kaneko, K., 2003. Hysteretic characteristics of Wells turbine for wave power conversion. Renew. Energy 28 (13), 2113–2127.

Kim, T.W., Kaneko, K., Setoguchi, T., Inoue, M., 1988. Aerodynamic performance of an impulse turbine with self-pitch-controlled guide vanes for wave power generator. In: Proceedings of the 1st KSME-JSME Thermal and Fluid Engineering Conference, Seoul, Korea, 2, pp. 133–137.

Mohamed, M.H., Janiga, G., Pap, E., Thévenin, D., 2011. Multi-objective optimization of the airfoil shape of Wells turbine used for wave energy conversion. Energy 36 (1), 438–446.

Mohamed, M.H., Shapaan, S., 2014. Numerical optimization of axial turbine with self pitch controlled blades used for wave energy conversion. J. Energy Res. 38 (5), 592–601.

Raghunathan, S., 1985. Performance of the Wells self-rectifying turbine. Aeronaut. J. 89 (1368), 369–379.

Raghunathan, S., 1995. The Wells air turbine for wave energy conversion. Prog. Aerosp. Sci. 31, 335–386.

Setoguchi, T., Santhakumar, S., Maeda, H., Takao, M., Kaneko, K., 2001. A review of impulse turbine for wave energy conversion. Renew. Energy 23, 261–292.

Setoguchi, T., Santhakumar, S., Takao, M., Kim, T.H., Kaneko, K., 2003a. A modified Wells turbine for wave energy conversion. Renew. Energy 28, 79–91.

Setoguchi, T., Takao, M., Itakura, K., Mohammad, M., Kaneko, K., 2003b. Effect of rotor geometry on the performance of Wells turbine. In: Proceedings of the 13th International Offshore and Polar Engineering Conference, Honolulu, Hawaii, USA, 1, pp. 374–381.

Takao, M., Kinoue, Y., Setoguchi, T., Kaneko, K., Nagata, S., 2006. Improvement of Wells turbine performance by means of end plate. Trans. Jpn. Soc. Mech. Eng. B 72, 2381–2385.

Takao, M., Setoguchi, T., 2012. Air turbines for wave energy conversion. Int. J. Rotating Mach. 1, 1–11.

Takao, M., Setoguchi, T., Kim, T.H., Kaneko, K., Inoue, M., 2001. The performance of a Wells turbine with 3D guide vanes. Int. J. Offshore Polar Eng. 11 (1), 72–76.

Thakker, A., Dhanasekaran, T.S., 2003. Computed effects of tip clearance on performance of impulse turbine for wave energy conversion. Renew. Energy 29 (4), 529–547.

Thakker, A., Dhanasekaran, T.S., 2005. Experimental and computational analysis on guide vane losses of impulse turbine for wave energy conversion. Renew. Energy 30 (9), 1359–1372.

Thakker, A., Dhanasekaran, T.S., Ryan, J., 2005. Experimental studies on effect of guide vane shape on performance of impulse turbine for wave energy conversion. Renew. Energy 30 (15), 2203–2219.